https://doi.org/10.5194/ar-2023-12
Preprint. Discussion started: 21 September 2023

AEROSOL Research Discussions

A comprehensive design schedule for electrosprayed thin films with different surface morphologies

Susan W. Karuga[1], Jan C. M. Marijnissen[2], Erik M. Kelder[3]

[1]Department of Electrical and Information Engineering, University of Nairobi, Nairobi, P.O Box 30197-00100, Kenya.
[2]Institute of Nuclear Science and Technology, University of Nairobi, Nairobi, P.O Box 30197-00100, Kenya.
[3]Department of Radiation Science and Technology, Delft University of Technology, Delft, P.O. Box 15, 2629 BJ Mekelweg, The Netherlands.

Correspondence to: Susan W. Karuga (swkaruga@uonbi.ac.ke)

Abstract. Electrospraying, a technique where a liquid jet breaks up into droplets under the influence of electrical forces, is outstanding because of its high deposition efficiency and ability to achieve thin films of different surface morphologies. Nowadays, the technique is applied in the deposition of thin films for nanoelectronics in Li-ion batteries, fuel cells and solar cells where performance of the deposited layers is determined by their morphologies. In this study, a literature survey has been conducted from which a comprehensive design schedule for electrosprayed thin films has been developed. In summary different porous and dense morphologies can be produced from the developed design schedule. Electrospray experiments have also been performed by altering different parameters as per the developed schedule. Using lithium salt precursor solutions, different thin films have been deposited on aluminium foil substrates and their characterization performed using scanning electron microscopy. The surface morphologies of the prepared thin films agree with the predictions of the developed design schedule.

1 Introduction

Electrospray is a technique in which a liquid jet is broken up into droplets in the presence of electrical forces. This study focuses on electrospraying in the cone-jet mode, therefore this mode is discussed in depth. The cone-jet mode is usually obtained when a precursor liquid is pumped through a nozzle at a low flow rate such that dripping is observed in the absence of an electric field. However, when an electric field is applied between the nozzle and the counter electrode and the electric field is increased instantaneously, other modes can be achieved as shown in Fig. 1. These modes include, intermittent cone-jet, spindle though not shown in Fig. 1, cone-jet and multiple jet modes (Cloupeau and Prunet-Foch, 1994; Swarbrick et al., 2006). Normally, the cone-jet mode is of interest because of its stability and capability to generate spherical monodisperse droplets which are smaller than the nozzle diameter (Joshi et al., 2021). As mentioned, the precursor solution is pumped through a nozzle with an electrical voltage applied between the nozzle and a ground electrode. The resulting electric field creates a charge on the meniscus of the liquid in the nozzle. Owing to the electric field and the surface charge, the liquid meniscus experiences an electric stress. This electric stress can overcome surface tension and shape the meniscus into a cone,

https://doi.org/10.5194/ar-2023-12
Preprint. Discussion started: 21 September 2023

AEROSOL Research Discussions

referred to as the Taylor cone, depending on the strength of the electric field and the liquid flow rate (Taylor, 1964). Charge carriers in the liquid consisting of ions are then accelerated towards the cone's apex. They collide with the surrounding liquid molecules causing them to also accelerate. Consequently, a thin liquid jet emerges from the cone's apex which breaks up into highly charged droplets.

In the past, several papers have reported on electrospray technique and they have shown that uniform thin films with different surface morphologies can be achieved. Nonetheless, the studies do not give a systematic way of designing the different surface morphologies and most outcomes are based on a trial-and-error method. Therefore, this study will consider the outcomes of related studies as obtained from literature to come up with a systematic way of designing thin films of different surface morphologies using electrospray technique.

2 Theory of Electrospray Technique

Typically, in an electrospray experiment charged droplets are generated and directed towards a counter electrode, which can be a selected substrate. Upon evaporation of the solvent in the generated droplets, particles are formed. To estimate the sizes of the droplets and particles formed in cone-jet mode, different authors have derived scaling laws. As it will be seen, electric current flowing through the liquid is a key parameter in the estimation of droplet and particle sizes (Yurteri et al., 2010). In the determination of the jet's electric current, Ganan-Calvo et al. (1997) presented two distinct profiles, namely flat and non-flat profiles. According to them, liquids with high viscosity and high conductivity have a flat radial profile of the axial liquid velocity in the jet while liquids with low conductivity and low viscosity have a non-flat velocity profile in the jet. To differentiate between these two categories of liquids, the same authors developed a dimensionless number (Eq. (1)) later referred to as the viscosity number (VN) by Hartman (1998).

$$VN = \left(\frac{\gamma^3 \varepsilon_0^2}{\mu^3 K^2 Q}\right)^{1/3} \quad (1)$$

where, γ is surface tension (N m^{-1}), ε_0 is electric permittivity of a vacuum (C^2 N^{-1} m^{-2}), μ is liquid absolute viscosity (Pa s), K is liquid conductivity (S m^{-1}) and Q is liquid flow rate (m^3 s^{-1}). For high viscosity and/or high conductivity the VN is relatively low. In practice, a flat radial velocity profile is assumed for viscosity numbers less than or equal to one, while a non-flat radial velocity profile is assumed for viscosity numbers greater than one. For a jet with a flat radial profile, Hartman et al. (1999) derived the equation for electric current as shown in Eq. (2).

https://doi.org/10.5194/ar-2023-12
Preprint. Discussion started: 21 September 2023

$$I^* = b(\gamma KQ)^{0.5} \quad (2)$$

where, I* is jet current for a flat radial profile of axial liquid velocity, b = 2.17 and the other parameters retain the same meaning as in Eq. (1). For liquids with a non-flat radial profile, Hartman (1998) derived a formula to calculate the electric current which was rewritten by Yurteri et al. (2010) in the form of Eq. (3).

$$I = 0.41I^* + \frac{0.24I^{*2}}{E_{z,max}KQ}(Ar_{j0.41}^2 + B) \quad (3)$$

where, I is jet current for a non-flat radial profile of the axial velocity, I* is jet current for a flat radial profile of the axial velocity and $E_{z,max}$, $r_{j0.41}$, A and B are all functions of known parameters. The other parameters retain the same meaning as in Eq. (1). Later, Yurteri et al. (2010) combined these formulas in the form of a ratio as a function of VN leading to Eq. (4).

$$I/I^* = (1 - 0.1 * VN^{0.45})^{-1} \quad (4)$$

Having calculated the jet's electric current, the mechanism by which droplets are formed during jet breakup is also important and must be considered when determining droplet sizes. This mechanism depends on the ratio of the electric normal stress to the surface tension stress on the liquid's surface. A low stress ratio (< 0.3) results in varicose breakup while a high stress ratio results in whipping breakup. In the former, main droplets of similar size are obtained, but in some cases, satellite or secondary droplets may also form, resulting in a bimodal size distribution. On the contrary, whipping breakup leads to a broad size distribution of the main droplets (Yurteri et al., 2010). For both mechanisms, Hartman et al. (2000) derived scaling laws for the main droplet size as shown below.

$$d_{d,varicose} = c_d\left(\frac{\rho\varepsilon_0 Q^4}{I^2}\right)^{1/6} \quad (5)$$

where $d_{d,varicose}$ is droplet diameter in varicose breakup regime, c_d is approximately 2, ρ is liquid density (kg m^{-3}), I is jet's electric current and the other parameters retain the same meaning as in Eq. (1). Yurteri et al. (2010) demonstrated that if the radial profile of the axial fluid velocity in the jet is flat, then the current scales according to Eq. (2) and Eq. (5) leads to Eq. (6).

$$d_{d,varicose} = \frac{c_d}{b^{1/3}}\left(\frac{\rho\varepsilon_0 Q^3}{\gamma K}\right)^{1/6} \quad (6)$$

By approximating the values of b and c_d to 2 (as already mentioned above), which gives only a small deviation, Yurteri et al. (2010) obtained Eq. (7).

https://doi.org/10.5194/ar-2023-12
Preprint. Discussion started: 21 September 2023

$$d_{d,varicose} = \left(\frac{16\rho\varepsilon_0 Q^3}{\gamma K}\right)^{1/6} \quad (7)$$

and in the whipping breakup regime, they obtained the droplet diameter from Eq. (8).

$$d_{d,whipping} = \left(0.8\frac{288\varepsilon_0\gamma Q^2}{I^2}\right)^{1/3} \quad (8)$$

where $d_{d,whipping}$ is droplet diameter in whipping breakup regime, γ is surface tension (N m^{-1}), Q is liquid flow rate (m^3 s^{-1}) and I is jet's electric current. To calculate the droplet size, both Eq. (7) and (8) are used and the smallest value obtained is assumed to be the correct value. Having determined the size of the main droplets using Eq. (7) or Eq. (8), particle size can be estimated from the main droplet size as shown in Eq. (9) (Yurteri et al., 2010).

$$d_p = \sqrt[3]{f\frac{\rho_{droplet}}{\rho_{particle}}}d_{droplet}^3 \quad (9)$$

where d_p is particle diameter, f is mass fraction of the dissolved material, $\rho_{droplet}$ is liquid density, $\rho_{droplet}$ is final particle density and $d_{droplet}$ is the droplet diameter. However, this is only true for non-porous and non-hollow particles.

It is also important to note that a stable cone-jet can only be achieved if electrospray is carried out in a limited voltage and flow rate window. The first quantitative description of this stability window was provided by Cloupeau and Prunet-Foch (1989). For selected liquid properties, this window is defined by a minimum flow rate (Q_{min}) and a maximum flow rate (Q_{max}). The former is the lowest flow rate at which a certain liquid can be sprayed in the cone-jet mode (Hartman, 1998) while the latter is the flow rate beyond which the cone-jet becomes unsteady. Due to the wide variety of complex issues around the maximum flow rate, there is no formula available to define it (Ganan-Calvo et al., 2018). However, several authors have developed formulas for calculating the minimum flow rate. Among them is Hartman (1998) who suggests that the minimum flow rate is given by Eq. (10).

$$Q_{min} \sim Q_0 = \frac{\varepsilon_0\gamma}{\rho K} \quad (10)$$

Alternatively, Scheideler and Chen (2014) identified different Q_{min} scaling laws for low (Eq. (11)) and high (Eq. (12)) viscous liquids.

$$Q_{min,low\ viscosity} \sim \frac{\varepsilon\gamma}{K\rho} \quad (11)$$

$$Q_{min,high\ viscosity} \sim \frac{\gamma D^2}{\mu} \quad (12)$$

In these equations Q_{min} is minimum flow rate (m^3 s^{-1}), ε is liquid permittivity, ε_0 is electric permittivity of a vacuum (C^2 N^{-1} m^{-2}), γ is liquid surface tension (N m^{-1}), K is liquid electrical conductivity (S m^{-1}), ρ is liquid density (kg m^{-3}), D is outer

https://doi.org/10.5194/ar-2023-12
Preprint. Discussion started: 21 September 2023

nozzle diameter (m) and μ is liquid viscosity (Pa s). Note that Eq. (11) by Scheideler and Chen (2014) is almost similar to Eq. (10) by Hartman (1998).

3 Development of the design schedule

This section discusses the effects of various electrospray parameters on surface morphology as obtained from literature.

3.1 Substrate Temperature

Essentially, when making films by electrospraying, charged droplets are produced from a precursor liquid and they are directed at a substrate of choice. A solid layer is then formed after the solvent has evaporated, and this process can be accelerated by heating the substrate. Usually, the substrate temperature is set to be above or below the solvent boiling point. Consequently, different surface morphologies can be achieved depending on the choice of solvent and substrate temperature (Perednis et al., 2005). While keeping other parameters constant heating the substrate to a temperature above the solvent boiling point, results in a dense layer. This is because the high temperature leads to evaporation of a big percentage of the solvent from the droplet surface. Consequently, the droplet size reduces but its overall electric charge remains constant and the Rayleigh limit is exceeded causing it to explode into many smaller droplets (Rahmanpour and Ebrahimi, 2017). The smaller droplets drift towards the substrate under electrostatic forces and they are expected to dry up into even smaller particles leading to a dense layer. Conversely, at relatively high flow rates the produced droplets are relatively big (Jo et al., 2014; Varga et al., 2010). According to Vercoulen (1995) such droplets are less likely to achieve Rayleigh break up and they dry up on the substrate to form relatively big particles that lead to a porous layer. At different substrate temperatures ranging from 170 to 230 °C, Wang et al., (2009) reported a decrease in pore size with increasing substrate temperature. They prepared porous reticular Fe_2O_3 films using a 0.005 M precursor in a mixed solvent of ethanol and 1,2-propylene glycol (boiling points of 78 °C and 188.2 °C respectively) at a flow rate of 2.4 mL h^{-1}.

3.2 Type of Solvent

While keeping other parameters constant, different surface morphologies can also be achieved with different solvents. For instance, Duong et al., (2013) studied six different alcohols and for the different solvents, they obtained different particle morphologies ranging from smooth spherical particles to collapsed shell morphology. They attributed the difference in particle morphologies to the fact that different solvents evaporate at different rates varying the droplet sizes. Larger droplets resulted in collapsed particles because of the increased mechanical instabilities. The effect of different solvents on film morphology was also reported by Lafont et al., (2012) who obtained a more porous film with 1-propanol than with ethanol (boiling points of 97 °C and 78 °C respectively) after electrospraying respective 0.1 M $LiNi_{0.5}Mn_{1.5}O_4$ precursors at a flow rate of 1 mL h^{-1} and a substrate temperature of 350 °C.

https://doi.org/10.5194/ar-2023-12
Preprint. Discussion started: 21 September 2023

3.3 Flow rate

It has to be noted that among other parameters, flow rate controls the droplet size hence the final particle size. However, flow rate is not an absolute parameter since it is influenced by other factors as shown in Eq. (10), Eq. (11) and Eq. (12). Among these factors, conductivity is the most prominent and its variation can lead to a wide range of droplet sizes. Unfortunately, most of these parameters are not given by the authors of the literature cited here. Nonetheless, if the range of conductivity values is not too big it does not tremendously influence the droplet diameter. This is because in the equation for droplet size, the conductivity appears as a power of 1⁄6 or 1⁄3. On the contrary, if the range of conductivities is big the effect on droplet size is significant (Joshi et al., 2013). It is also important to know which flow rates can achieve the cone-jet mode. This is defined by a minimum flow rate (Eq. (10)) and a maximum flow rate and they form an operational window. Therefore, for future research it is recommended that all the involved precursor liquid parameters should be measured and mentioned. At a constant conductivity, low flow rate produces relatively small droplets hence small particles while high flow rate produces relatively big droplets that dry up into big particles. From the works of Kavadiya et al. (2017), electrospraying $CH_3NH_3PbI_3$ perovskite precursor (14 mg mL^{-1}) in isopropyl alcohol (boiling point of 82.5 °C) at flow rates of 0.03, 0.06, 0.09, 0.12 and 0.15 mL h^{-1} at room temperature led to droplets of diameters 505.88, 635.9, 726.94, 799.33 and 860.41 nm respectively and their reported evaporation times were 17.84, 28.22, 36.90, 44.64 and 51.73 µs respectively. The measured particle sizes were 75.36, 77.00, 109.23, 116.31 and 113.43 nm respectively. Smaller particle sizes were achieved at lower flow rates and they led to the production of smooth uniform films. However, as flow rate increased (above 0.06 mL h^{-1}) larger particles were obtained leading to increased film roughness. According to Hong et al. (2017), small droplets have a high rate of solvent evaporation leading to a particulate rough film while big droplets have a low rate of solvent evaporation leading to an uneven film with pinholes. Therefore, an intermediate droplet size is required in order to obtain a uniform dense film. They achieved this by electrospraying 30 % wt $MAPbI_3$ perovskite liquid precursor in DMSO (boiling point of 189 °C) at a flow rate of 0.05 mL h^{-1} and a substrate temperature of 65 °C for 2 min. Different morphological effects based on flow rate were also demonstrated by Ma and Qin (2005) during the electrospray of 0.02 M $LiFePO_4$ precursor solution in a mixed solvent of ethanol, glycol and butyl carbitol (boiling points of 78 °C, 197 °C and 231 °C respectively) at a substrate temperature of 120 °C. At a flow rate of 0.5 mL h^{-1}, the generated particles were big (> 400 nm) and they aggregated to form a porous morphology. On the contrary, at a flow rate of 0.05 mL h^{-1} the generated particles were smaller (< 100 nm) and they formed a uniform dense film. Also, Yu, Shui, and Chen (2006) reported a porous film with aggregated particles at a flow rate of 4 mL h^{-1} using 0.02 M $LiCoO_2$ precursor in a mixed solvent of ethanol and glycol (boiling points of 78 °C and 197 °C respectively) at a substrate temperature of 350 °C deposited for 50 min.

3.4 Concentration

Another factor that influences surface morphology is the precursor liquid concentration. According to Gürbüz et al. (2016), an increase in concentration increases the film thickness which affects morphology. In their study, they electrosprayed SnO_2

https://doi.org/10.5194/ar-2023-12
Preprint. Discussion started: 21 September 2023

precursor in ethanol (boiling point of 78 °C) at a substrate temperature of 250 °C for 1 h. Precursor concentrations were varied from 0.05 M to 0.2 M but flow rate was kept constant at 7.2 mL h^{-1}. A crack free film was obtained from the 0.05 M precursor while a cracked film was obtained after increasing the concentration to 0.2 M. At high concentration, cracking was attributed to the non-uniform drying rate between the top and bottom layers of the thick film. Also, Bailly et al. (2012) reported a cracked film after electrospraying 0.1 M YSZ precursor in a mixed solvent of ethanol and butyl carbitol (boiling points of 78 °C and 231 °C respectively) at a substrate temperature of 400 °C and a flow rate of 0.5 mL h^{-1} for 1 h. In another study, Joshi et al. (2013) reported a dense film from a low concentration (0.05 M) $SnCl_4.5H_2O$ precursor in propylene glycol (boiling point of 188.2 °C) at a flow rate of 0.04 mL h^{-1} and a substrate temperature of 70 °C for 1 h.

3.5 Deposition time

Deposition time is a very important parameter not only in determining the layer thickness but also the surface morphology. Joshi et al. (2021) mentioned that by increasing the deposition time, film morphology can change from dense to porous. In a short deposition time the film is thin and the droplets get into direct contact with the heated substrate. With increasing time, the film thickens and the substrate surface is completely covered causing consecutive landing droplets to experience varying contact angles that alter the surface morphology. The effects of deposition time on surface morphology were investigated by Gürbüz et al. (2016), who deposited 0.05 M SnO_2 film from an ethanol precursor (boiling point of 78 °C) at a flow rate of 7.2 mL h^{-1} and at a substrate temperature of 250 °C for various time intervals. At 20 min, they observed that the substrate was sparsely covered because of the small number of liquid droplets. At 60 min, a lot of droplets had been deposited on the substrate covering the whole surface and it led to a homogenous porous film. After electrospraying a 0.1 M YSZ precursor in a mixed solvent of ethanol and butyl carbitol (boiling points of 78 °C and 231 °C respectively) at a flow rate of 0.5 mL h^{-1} and a substrate temperature of 400 °C, Neagu et al. (2006) reported a dense coating at 1 h and rough coatings at 4 and 12 h. They attributed the surface roughness to preferential landing of the droplets that occurred at longer deposition periods. For Maršálek et al. (2015), they prepared manganese oxide layers from a 0.02 M precursor in a mixed solvent of ethanol and water (boiling points of 78 °C and 100 °C respectively) at a flow rate of 1 mL h^{-1} and a substrate temperature of 200 °C. Deposition times between 10 and 30 min yielded relatively compact and thin layers while longer periods led to formation of agglomerates. In the study by Joshi et al. (2015), they obtained porous films using 0.1 M Bi_2WO_6 precursor in propylene glycol (boiling point of 188.2 °C) deposited at a substrate temperature of 120 °C and a flow rate of 0.04 mL h^{-1} for 80 min. They reported increased film porosity with deposition time. In another study, Joshi et al. (2012) obtained a dense film using 0.3 M ZnO precursor solutions in propylene glycol (boiling point of 188.2 °C) at a flow rate of 0.075 mL h^{-1} and a substrate temperature of 200 °C for 30 min. At short deposition times (10, 20, 40 and 60 min), Yoon et al. (2016) obtained uniform compact films from WO_3 precursor in mixed solvent of polyethylene and ethanol (boiling points of 200 °C and 78 °C respectively) at a flow rate of 0.08 mL h^{-1} and a substrate temperature of 80 °C. In other studies, long deposition time led to a porous reticular morphology. As indicated by Koike and Tatsumi (2005; 2007), droplets spread gradually on the substrate surface and the temperature at the droplet edge is higher than at its centre. Therefore, the solvent at the droplet edge

https://doi.org/10.5194/ar-2023-12
Preprint. Discussion started: 21 September 2023

evaporates faster than at its centre. This process leads to ring-shaped nucleation and precipitation that forms a reticular morphology on the substrate. An example is Ma et al. (2014) who electrosprayed 0.1 M MnO precursor in 1,2-dihydroxypropane (boiling point of 188.2 °C) at a substrate temperature of 240 °C and a flow rate of 1.5 mL h^{-1} for 3 h. Another example is J. Yuan et al. (2017) using 2 mM $CoMn_2O_4$ precursor in a mixture of ethanol and 1,2-propanediol (boiling points of 78 °C and 188.2 °C respectively) at a substrate temperature of 250 °C and a flow rate of 2 mL h^{-1} for 4 h. Also T. Yuan et al. (2017) using 0.01 M $CoMn_2O_4$ precursor in 1,2-propanediol (boiling point of 188.2 °C) at a substrate temperature of 200 °C and a flow rate of 2 mL h^{-1} for 3 h. The porosity of the film was observed to increase with deposition time as demonstrated by Wang et al. (2011) who used a 0.03 M V_2O_5 precursor in a solvent mixture of water, ethanol and 1,2 propylene glycol (boiling points of 100 °C, 78 °C and 188.2 °C) at a flow rate of 72 mL h^{-1} and a substrate temperature of 260 °C for deposition times ranging from 4 to 12 h.

Conclusively, the results of the mentioned researchers have been used to make a design schedule, as shown in Table 1. Note that a study by Joshi et al. (2021) gives much more examples but cannot be fitted in the schedule since not all parameters are indicated.

4 Experimental Work

The experiments were carried out using the electrospray set up shown in Fig. 2. It consists of a heated substrate holder, a nozzle (EFD ULTRA), a high voltage power supply (FUG HCN14-12500) connected to the nozzle, a syringe pump (KD Scientific 100) where a precursor solution contained in a syringe is fed in a controlled flow rate via a chemically-resistant hose (Watson-Marlow) to the nozzle and a temperature controller connected to the substrate holder. The nozzle is held on a movable table which allows the adjustment of nozzle to substrate distance. The lithium nickel manganese oxide ($LiNi_{0.5}Mn_{1.5}O_4$, LNMO) precursor solutions were prepared by dissolving stoichiometric amounts of reagent grade lithium nitrate ($LiNO_3$), manganese nitrate ($Mn(NO_3)_2{\cdot}4H_2O$) and nickel nitrate ($Ni(NO_3)_2{\cdot}6H_2O$) in 2-propanol (boiling point of 82.5 °C). The lithium chloride (LiCl) precursor solutions were prepared by dissolving reagent grade lithium chloride (LiCl) in dimethyl sulfoxide (DMSO) (boiling point of 189 °C). Different precursor solutions were pumped through the syringe at selected flow rates and the nozzle to substrate distance was 2 or 3 cm. For each experiment, the precursor was sprayed through a metallic nozzle of 1.54 mm internal diameter. To create an electric field, the substrate holder was grounded while a high voltage was applied on the metallic nozzle. The voltage applied on the nozzle was adjusted for each experiment to yield a steady cone-jet. At this point the liquid meniscus on the nozzle acquired the shape of a cone that did not relax back to a normal droplet shape. After spraying for a selected duration, a thin film was deposited on a heated aluminium foil substrate at a selected temperature to evaporate the solvent. The resulting surface morphologies for the films generated from different experiments were analyzed using a scanning electron microscope (JEOL JSM-6010LA) operated at voltages of 5 - 15 kV.

https://doi.org/10.5194/ar-2023-12
Preprint. Discussion started: 21 September 2023

5 Results

Fig. 3 shows a porous film with agglomerates obtained when a high concentration precursor solution was sprayed on a substrate at a high temperature for a long time at a high flow rate.

Fig. 4 shows a porous reticular film obtained when a high concentration precursor solution was sprayed on a substrate at a low temperature for a long time at a high flow rate.

Fig. 5 shows a dense particulate film obtained when a high concentration precursor solution was sprayed on a substrate at a low temperature for a short time at a high flow rate. The higher boiling point was used to define low temperature difference.

Fig. 6 shows a porous agglomerates film obtained when a high concentration precursor solution was sprayed on a substrate at a low temperature for a long time at a low flow rate.

Fig. 7 shows a porous reticular film obtained when a low concentration precursor solution was sprayed on a substrate at a high temperature for a long time at a high flow rate.

of 2 mL h^{-1} and a substrate temperature of 350 °C for 2 h.

Fig. 8 shows a porous reticular film obtained when a low concentration precursor solution was sprayed on a substrate at a low temperature for a long time at a high flow rate. Comparing Fig. 7 and Fig. 8, it is clear that the film becomes more compact with an increase in substrate temperature.

Fig. 9 shows a porous agglomerates film obtained when a high concentration precursor solution was sprayed on a substrate at a high temperature for a long time at a low flow rate.

Fig. 10 shows a dense particulate film obtained when a low concentration precursor solution was sprayed on a substrate at a low temperature for a short time at a low flow rate.

6 Conclusion

From this study, a comprehensive design schedule for electrosprayed thin films has been developed. From the schedule, thin films of different morphologies can be prepared by controlling the key parameters identified as; precursor concentration, precursor flow rate or actually droplet size, substrate temperature and deposition time. Therefore, these parameters must be determined and indicated for each electrospray experiment. Thin films deposited in this study agree with the developed design schedule and they show that porous and dense morphologies can be produced. Therefore, electrospraying in the cone-jet mode is a versatile method for designing/producing thin films with desired surface morphologies.

Data availability

All raw data can be provided by the corresponding authors upon request.

https://doi.org/10.5194/ar-2023-12
Preprint. Discussion started: 21 September 2023

Author contributions

SWK and JCMM designed the research; SWK performed the experiments; EMK and SWK analyzed the thin films; SWK wrote the manuscript draft; JCMM and EMK reviewed and edited the manuscript; JCMM and EMK supervised the work. All authors made substantial contributions to this work.

Competing interests

The authors declare that they have no conflict of interest.

Acknowledgements

We acknowledge the International Science Programme at Uppsala University in Sweden for their financial support. The authors would also like to thank Walter Legerstee for his support during SEM measurements.

Financial support

This work was supported by the International Science Programme at Uppsala University in Sweden (Project KEN 01/2, 2017-2021).

References

Bailly, N., Georges, S. and Djurado, E.: Elaboration and electrical characterization of electrosprayed YSZ thin films for intermediate temperature-solid oxide fuel cells (IT-SOFC), Solid State Ion. 222–223, 17, doi 10.1016/j.ssi.2012.06.020, 2012.

Cloupeau, M. and Prunet-Foch, B.: Electrostatic Spraying of Liquids in Cone-Jet Mode. J. Electrost. 22, 135-159, doi: 10.1016/0304-3886(89)90081-8, 1989.

Cloupeau, M. and Prunet-Foch, B.: Electrohydrodynamic spraying functioning modes: a critical review. J. Aerosol Sci. 25, 6, 1021-1036, doi: 10.1016/0021-8502(94)90199-6, 1994.

Duong, A. D., Sharma, S., Peine, K. J., Gupta, G., Satoskar, A. R., Bachelder, E. M., Wyslouzil, B. E. and Ainslie, K. M.: Electrospray Encapsulation of Toll-Like Receptor Agonist Resiquimod in Polymer Microparticles for the Treatment of Visceral Leishmaniasis. Mol. Pharmaceutics 10, 3, 1045-55, doi: 10.1021/mp3005098, 2013.

Ganan-Calvo, A. M., Davila, J. and Barrero, A.: Current and Droplet Size in the Electrospraying of Liquids. Scaling Laws. J. Aerosol Sci. 28, 2, 249-275, doi: 10.1016/S0021-8502(96)00433-8, 1997.

Ganan-Calvo, A. M., López-Herrera, J. M., Herrada, M. A., Ramos, A. and Montaner, J. M.: Review on the physics electrospray: from electrokinetics to the operating conditions of single and coaxial Taylor cone-jets, and AC electrospray. J. Aerosol Sci. 125: 32-56, doi: 10.1016/j.jaerosci.2018.05.002, 2018.

https://doi.org/10.5194/ar-2023-12
Preprint. Discussion started: 21 September 2023

Gürbüz, M., Günkaya, G. and Doğan. A.: Electrospray deposition of SnO_2 films from precursor solution. Surf. Eng. 32, 10, 725-32. doi: 10.1080/02670844.2015.1108048, 2016.

Hartman, R. P. A.: Electrohydrodynamic Atomization in the Cone-Jet Mode. From Physical Modelling to Powder Production. PhD Thesis, Delft University of Technology, ISBN: 90-9012086-6, 1998.

Hartman, R. P. A., Brunner, D. J., Camelot, D. M. A., Marijnissen, J. C. M. and Scarlett, B.: Electrohydrodynamic Atomization in the Cone-Jet Mode Physical Modeling of the Liquid Cone and Jet. J. Aerosol Sci. 30, 7, 823-49, doi: 10.1016/S0021-8502(99)00033-6, 1999.

Hartman, R. P. A., Brunner, D. J., Camelot, D. M. A., Marijnissen, J. C. M and Scarlett, B.: Jet Break-Up in Electrohydrodynamic Atomization in the Cone-Jet Mode. J. Aerosol Sci. 31, 1, 65-95, doi: 10.1016/S0021-8502(99)00034-8, 2000.

Hong, S. C., Lee, G., Ha, K., Yoon, J., Ahn, N., Cho, W., Park, M. and Choi, M.: Precise Morphology Control and Continuous Fabrication of Perovskite Solar Cells Using Droplet-Controllable Electrospray Coating System. ACS Appl. Mater. Interfaces 9, 9, 7879–7884, doi: 10.1021/acsami.6b15095, 2017.

Jo, Y. J., Kim, Y. H., Jo, Y. H., Seong, J. G., Chang, S. Y., Van Tyne, C. J. and Lee, W. H.: Microporous Ti Implant Compact Coated with Hydroxyapatite Produced by Electro-Discharge-Sintering and Electrostatic-Spray-Deposition. J. Nanosci. Nanotechnol. 14, 8439-44, doi: 10.1166/jnn.2014.9933, 2014.

Joshi, B., Samuel, E. Kim, Y., Yarin, A. L., Swihart, M. T. and Yoon, S. S.: Electrostatically Sprayed Nanostructured Electrodes for Energy Conversion and Storage Devices. Adv. Funct. Mater. 31, 14, 2008181, doi: 10.1002/adfm.202008181, 2021.

Joshi, B., Yoon, H. Kim, H. Kim, M. Mali, M. G. Al-Deyab, S. S. and Yoon, S. S.: Heterojunction photoanodes for solar water splitting using chemical-bath-deposited In2O3 micro-cubes and electro-sprayed Bi_2WO_6 textured nanopillars. RSC Adv. 5, 104, 85323–8, doi: 10.1039/C5RA16833C, 2015.

Joshi, B. N., Yoon, H. and Yoon, S. S.: Structural, optical and electrical properties of tin oxide thin films by electrostatic spray deposition. J. Electrost. 71, 1, 48–52, doi: 10.1016/j.elstat.2012.11.024, 2013.

Joshi, B. N., Yoon, H. Kim, H. Y., Oh, J. H., Seong, T. Y. James, S. C. and Yoon, S. S.: Effect of Zinc Acetate Concentration on Structural, Optical and Electrical Properties of ZnO Thin Films Deposited by Electrostatic Spray on an ITO Substrate. J. Electroch. Soc. 159 (8): H716–21, doi: 10.1149/2.077208jes, 2012.

Kavadiya, S., Niedzwiedzki, D. M., Huang, S. and Biswas, P.: Electrospray-Assisted Fabrication of Moisture-Resistant and Highly Stable Perovskite Solar Cells at Ambient Conditions. Adv. Energy Mater. 1700210, doi: 10.1002/aenm.201700210, 2017.

Koike, S. and Tatsumi, K.: Preparation and morphology of three-dimensional structured $LiMn_2O_4$ films. J. Power Sources 146, 1-2, 241–44, doi: 10.1016/j.jpowsour.2005.03.038, 2005.

Koike, S. and Tatsumi, K.: Preparation and performances of highly porous layered $LiCoO_2$ films for lithium batteries. J. Power Sources 174 (2): 976–80, doi: 10.1016/j.jpowsour.2007.06.219, 2007.

https://doi.org/10.5194/ar-2023-12
Preprint. Discussion started: 21 September 2023

Lafont, U., Anastasopol, A., Garcia-Tamayo, E. and Kelder, E.: Electrostatic spray pyrolysis of LiNi0.5Mn1.5O4 films for 3D Li-ion microbatteries. Thin Solid Films 520: 3464-71, doi: 10.1016/j.tsf.2011.12.041, 2012.

Li, X., Dhanabalan, A. and Wang, C.: Enhanced electrochemical performance of porous NiO–Ni nanocomposite anode for lithium ion batteries. J. Power Sources 196, 9625-9630, doi: 10.1016/j.jpowsour.2011.06.097, 2011.

Ma, J., and Qin, Q.: Electrochemical performance of nanocrystalline $LiMPO_4$ thin-films prepared by electrostatic spray deposition. J. Power Sources 148, 66-71, doi: 10.1016/j.jpowsour.2005.01.041, 2005.

Ma, X. H., Wan, Q. Y., Huang, X., Ding, C. X., Jin, Y., Guan, Y. B. and Chen, C. H. Synthesis of three-dimensionally porous MnO thin films for lithium-ion batteries by improved Electrostatic Spray Deposition technique. Electrochim. Acta 121, 15-20, doi: 10.1016/j.electacta.2013.12.004, 2014.

Maršálek, J., Chmelař, J. Pocedič, J. and Kosek, J.: Morphological and electrochemical study of Mn_xO_y nanoparticle layers prepared by electrospraying. Chem. Eng. Sci. 123: 292–99, doi: 10.1016/j.ces.2014.10.044, 2015.

Neagu, R., Djurado, E., Ortega, L. and Pagnier, T.: ZrO_2-based thin films synthesized by electrostatic spray deposition: Effect of post-deposition thermal treatments. Solid State Ion. 177, 17-18, 1443–1449, doi: 10.1016/j.ssi.2006.06.024, 2006.

Perednis, D., Wilhelm, O., Pratsinis, S. E. and Gauckler, L. J.: Morphology and deposition of thin yttria-stabilized zirconia films using spray pyrolysis. Thin Solid Films 474: 84-95, doi: 10.1016/j.tsf.2004.08.014, 2005.

Rahmanpour, M., and Ebrahimi, R.: Numerical Simulation of Highly Charged Droplets Dynamics with Primary Break-up in Electrospray at Sub Rayleigh Limit. J. Appl. Fluid Mech. 10, 2, 541-50, doi: 10.18869/ACADPUB.JAFM.73.239.26186, 2017.

Scheideler, W. J. and Chen, C. The minimum flow rate scaling of Taylor cone-jets issued from a nozzle. Appl. Phys Lett. 104: 024103, doi: 10.1063/1.4862263, 2014.

Swarbrick, J. C., Taylor, J. B. and O'Shea, J. N.: Electrospray deposition in vacuum, Appl. Surf. Sci. 252, 15, 5622-5626, doi: 10.1016/j.apsusc.2005.12.025, 2006.

Taylor, G. I.: Disintegration of Water Drops in An Electric Field. Proc. R. Soc. A280: 383-97, doi: 10.1098/rspa.1964.0151, 1964.

Varga, A., Brunelli, N. A., Louie, M. W., Giapis, K. P. and Haile, S. M. Composite nanostructured solid-acid fuel-cell electrodes via electrospray deposition. J. Mater. Chem. 20, 30, 6309, doi: 10.1039/C0JM00216J, 2010.

Vercoulen, P. H. W.: Electrostatic Processing of Particles: A tool in particle technology. PhD Thesis, Delft University of Technology, ISBN: 90-9008193-3, 1995.

Verdoold, S., Agostinho, L. L. F., Yurteri, C. U. and Marijnissen, J. C. M. A generic electrospray classification. J. Aerosol Sci. 67, 87-103, doi: 10.1016/j.jaerosci.2013.09.008, 2014.

Wang, S., Li, S., Sun, Y., Feng, X. and Chen, C. Three-dimensional porous V_2O_5 cathode with ultra high rate capability. Energy Environ. Sci. 4, 8, 2854-2857, doi: 10.1039/c1ee01172c, 2011.

https://doi.org/10.5194/ar-2023-12
Preprint. Discussion started: 21 September 2023

Wang, L., Xu, H. W., Chen, P. C., Zhang, D. W., Ding, C. X. and Chen, C. H.: Electrostatic spray deposition of porous Fe_2O_3 thin films as anode material with improved electrochemical performance for lithium–ion batteries. J. Power Sources 193: 846-850, doi: 10.1016/j.jpowsour.2009.03.063, 2009.

Yoon, H., Mali, M. G., Kim, M., Al-Deyab, S. S. and Yoon, S. S.: Electrostatic spray deposition of transparent tungsten oxide thin-film photoanodes for solar water splitting. Catal. Today, 260, 89–94, doi: 10.1016/j.cattod.2015.03.037, 2016.

Yu, Y., Shui, J. L. and Chen, C. H.: Electrostatic spray deposition of spinel $Li_4Ti_5O_{12}$ thin films for rechargeable lithium batteries. Solid State Commun. 135: 485-89, doi: 10.1016/j.ssc.2005.05.045, 2005.

Yu, Y., Shui, J. L., Jin, Y. and Chen, C. H.: Electrochemical performance of nano-SiO_2 modified $LiCoO_2$ thin films fabricated by electrostatic spray deposition (ESD). Electrochim. Acta 51: 3292-96, doi: 10.1016/j.electacta.2005.09.021, 2006.

Yuan, J., Chen, C., Hao, Y., Zhang, X., Agrawal, R., Wang, C., Li, X., Hao, Y., Liu, B., Li, Q. and Xie, Y.: Three-dimensionally porous $CoMn_2O_4$ thin films grown on Ni foams for high-performance lithium-ion battery anodes. J. Mater. Sci. 52: 5751-58, doi: 10.1007/s10853-017-0810-6, 2017.

Yuan, T., Jiang, Y., Wang, Q., Pan, B. and Yan, M.: Pseudocapacitance-Enhanced High-Rate Lithium Storage in “Honeycomb”-like Mn_2O_3 Anodes. ChemElectroChem 4, 3, 565–569, doi: 10.1002/celc.201600588, 2017.

Yurteri, C. U., Hartman, R. P. A. and Marijnissen, J. C. M.: Producing Pharmaceutical Particles via Electrospraying with an emphasis on Nano and Nano structured Particles - A Review. KONA Powder Part. J. 28, 91-115, doi: 10.14356/kona.2010010, 2010.

https://doi.org/10.5194/ar-2023-12
Preprint. Discussion started: 21 September 2023

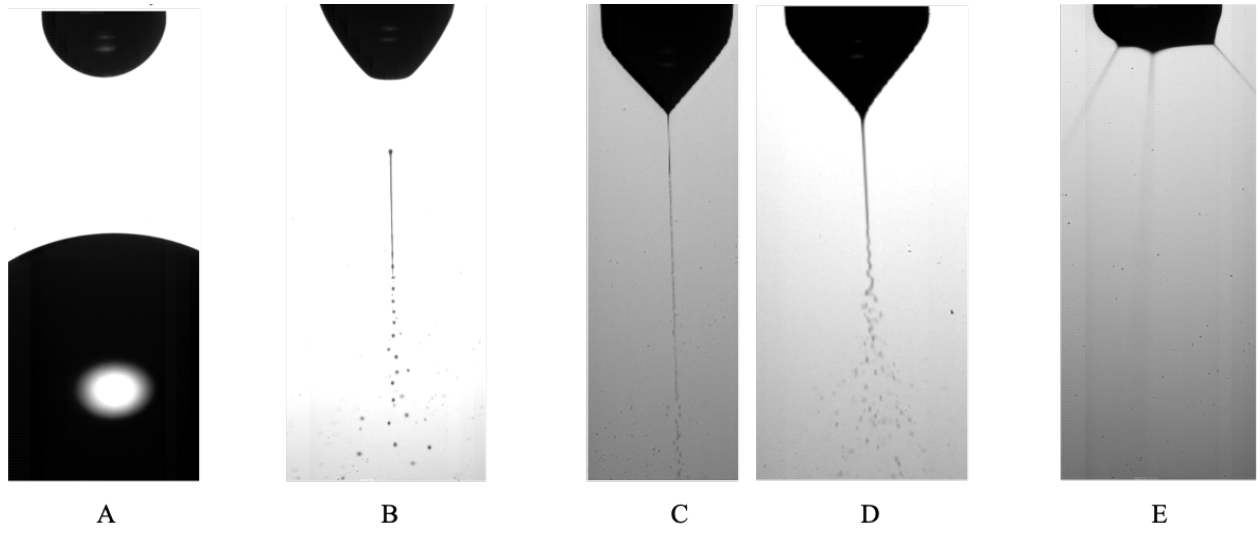

Figure 1: Examples of electrospray modes. A. Dripping, B. Intermittent cone-jet, C. Cone-jet, varicose breakup, D. Cone-jet, whipping breakup and E. Multiple-jet. Images reproduced with permission from Verdoold et al., 2014 and Yurteri et al., 2010.

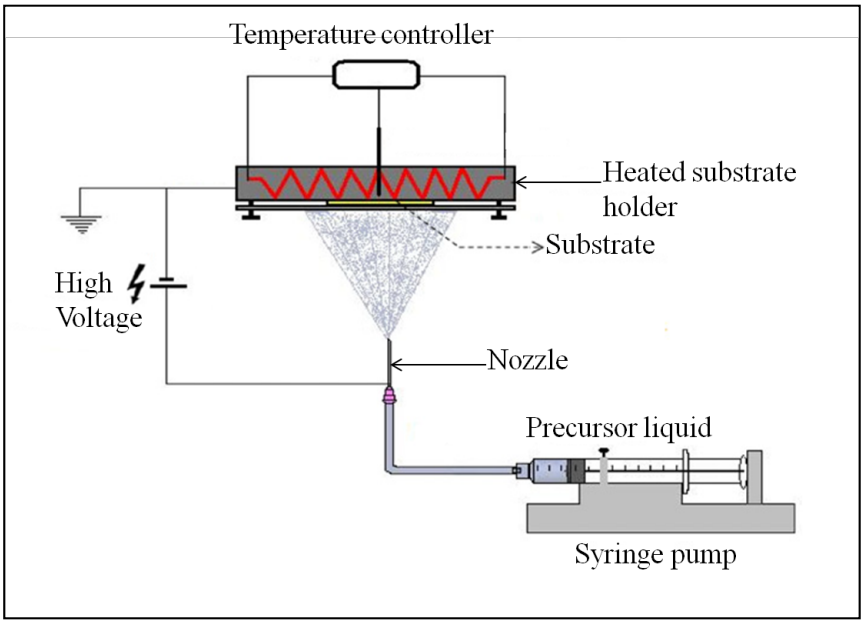

Figure 2: Schematics of the electrospray setup used in this study. Reproduced with permission from Li et al., 2011.

https://doi.org/10.5194/ar-2023-12
Preprint. Discussion started: 21 September 2023

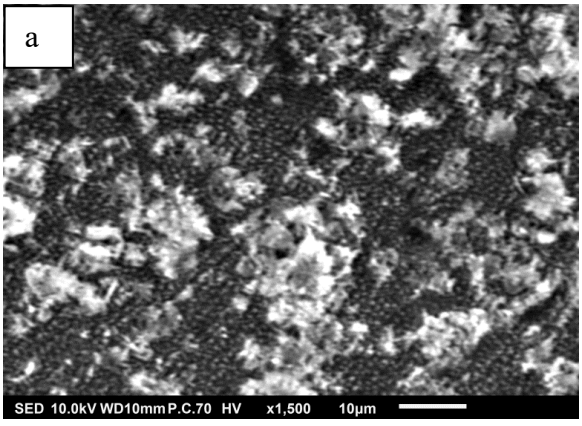

Figure 3: SEM image of a thin film generated by electrospraying 0.1 M LNMO precursor in 2-propanol at a flow rate of 1 mL h^{-1} and a substrate temperature of 200 °C for 3 h.

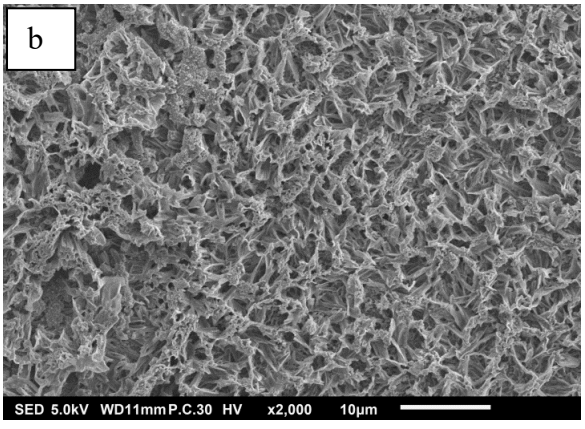

Figure 4: SEM image of a thin film generated by electrospraying 1 M LNMO precursor in 2-propanol at a flow rate of 2 mL h^{-1} and a substrate temperature of 100 °C for 3 h.

https://doi.org/10.5194/ar-2023-12
Preprint. Discussion started: 21 September 2023

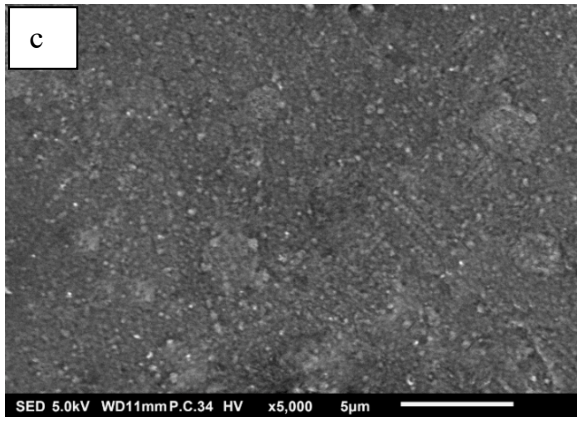

Figure 5: SEM image of thin film generated by electrospray of 0.5 M LNMO precursor in 2-propanol and ethylene glycol at a flow rate of 2 mL h^{-1} and a substrate temperature of 200 °C for 1 h.

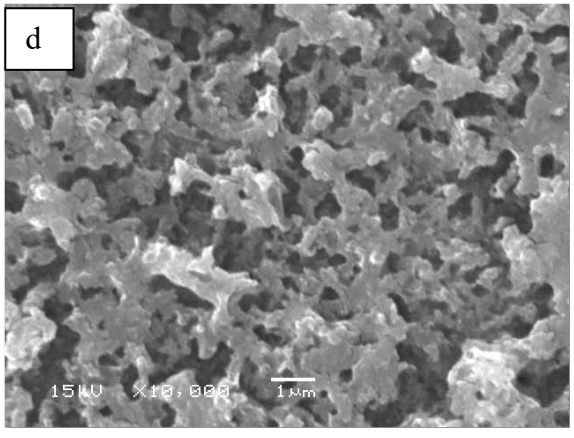

Figure 6: SEM image of thin film generated by electrospray of 1 M LiCl precursor in DMSO (boiling point of 189 °C) at a flow rate of 0.4 mL h^{-1} and a substrate temperature of 200 °C for 7 h.

https://doi.org/10.5194/ar-2023-12
Preprint. Discussion started: 21 September 2023

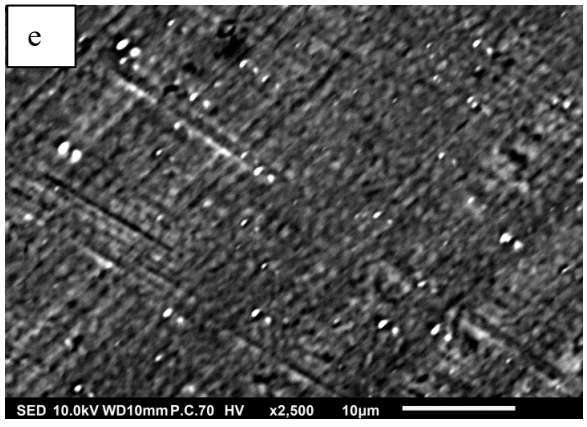

Figure 7: SEM image of a thin film generated by electrospray using 0.0375 M LNMO precursor in 2-propanol at a flow rate of 2 mL h^{-1} and a substrate temperature of 350 °C for 2 h.

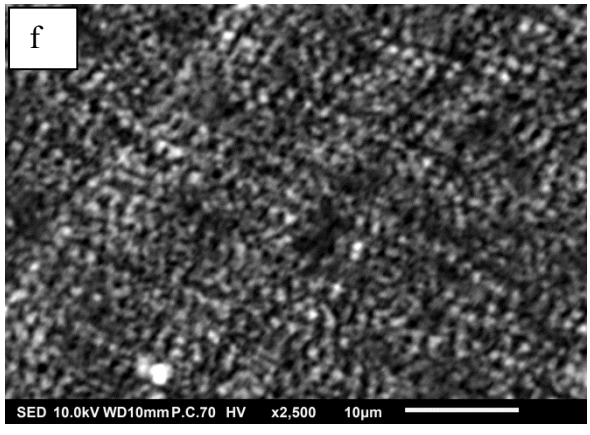

Figure 8: SEM image of a thin film generated by electrospray using 0.0375 M LNMO precursor in 2-propanol at a flow rate of 2 mL h^{-1} and a substrate temperature of 100 °C for 2 h.

https://doi.org/10.5194/ar-2023-12
Preprint. Discussion started: 21 September 2023

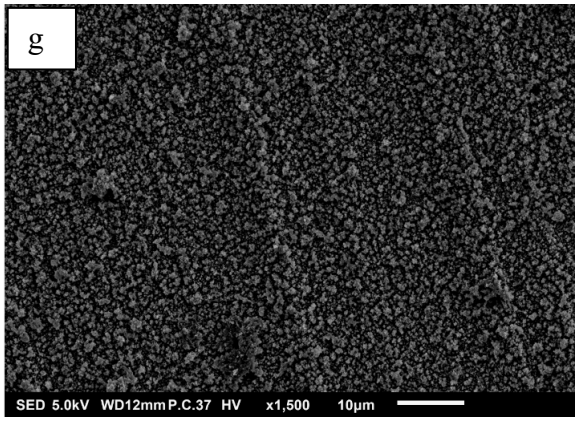

Figure 9: SEM image of thin film generated by electrospray of 0.3 M LNMO precursor in 2-propanol at a flow rate of 0.5 mL h^{-1} and a substrate temperature of 200 °C for 3 h.

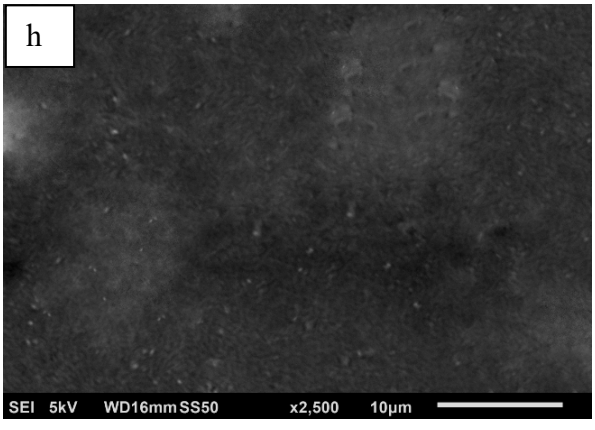

Figure 10: SEM image of thin film generated by electrospray of 0.05 M LiCl precursor in DMSO at a flow rate of 0.4 mL h^{-1} and a substrate temperature of 200 °C for 1 h.

https://doi.org/10.5194/ar-2023-12
Preprint. Discussion started: 21 September 2023

AEROSOL Research Discussions

Table 1: A design schedule showing how to obtain different surface morphologies by altering experimental and liquid parameters.

Experimental/precursor liquid parameters				Film morphology	References
High Concentration (≥ 0.1M) *[a]	High Flow rate*[b]	High substrate temperature*[c]	Long deposition time*[e]	Porous: agglomerates	Perednis et al., 2005
			Short deposition time*[f]	Porous: cracked film	Gürbüz et al., 2016; Bailly et al., 2012
		Low substrate temperature*[d]	Long deposition time	Porous: reticular	Ma et al., 2014
			Short deposition time	Dense: particulate	Perednis et al., 2005; Varga et al., 2010; Joshi et al., 2012
	Low Flow rate *[b]	High substrate temperature	Long deposition time	Porous: agglomerates	Neagu et al., 2006; Lafont et al., 2012
			Short deposition time	Dense: particulate	Neagu et al., 2006; Bailly et al., 2012
		Low substrate temperature	Long deposition time	Porous: agglomerates	Joshi et al., 2015
			Short deposition time	Dense: particulate	Yoon et al., 2016
Low Concentration (< 0.1M)	High Flow rate	High substrate temperature	Long deposition time	Porous: reticular	Wang et al., 2011; J. Yuan et al., 2017
			Short deposition time	Porous: broccoli-like agglomerates	Yu et al., 2006; Varga et al., 2010; Gürbüz et al., (2016)
		Low substrate temperature	Long deposition time	Porous: reticular	T. Yuan et al., 2017; Wang et al., 2011; Wang et al., 2009
			Short deposition	Porous:	Hong et al., 2017;

https://doi.org/10.5194/ar-2023-12
Preprint. Discussion started: 21 September 2023

			time	particulate	Kavadiya et al., 2017; Jo et al., 2014; Ma and Qin, 2005
	Low Flow rate	High substrate temperature	Long deposition time	Porous: agglomerate	Maršálek et al., 2015
			Short deposition time	Dense: particulate	Maršálek et al., 2015
		Low substrate temperature	Long deposition time	Porous: reticular	Koike and Tatsumi, 2005; Koike and Tatsumi, 2007
			Short deposition time	Dense: particulate	Hong et al., 2017; Kavadiya et al., 2017; Ma and Qin, 2005; Joshi et al., 2013

[*a]The concentration limit applies to the liquids used in this study. [*b]Whether flow rate is high or low is relative and depends on the droplet size. From our experiments, high flow rates result in big droplets ≥ 1 µm while low flow rates result in small droplets < 1 µm [*c]High substrate temperature is a value above the solvent boiling point with 55 °C or more. [*d]Low substrate temperature is a value below the solvent boiling point or slightly above solvent boiling point (with less than 55 °C). For the mixed solvents the boiling point of the liquid with the highest boiling point was used in the approximation of low or high substrate temperature. [*e]Long deposition time is > 1 h. [*f]Short deposition time is ≤ 1h.

https://doi.org/10.5194/ar-2023-12
Preprint. Discussion started: 21 September 2023

AEROSOL Research Discussions

Table 2: Parameters for different experiments.

Experiment number	Precursor solution	nozzle to substrate distance (cm)	Flow rate (mL h^{-1})	Droplet size (µm)	Duration (hours)	Substrate temperature (°C)	Solvent boiling point (°C)
a	0.1 M LNMO in 2-propanol	3	1	1.26	2	200	82.5
b	1 M LNMO precursor in 2-propanol	3	2	1.11	3	100	82.5
c	0.5 M LNMO in 2-propanol and ethylene glycol (1:1)	3	2	1.19	1	200	82.5 – 197
d	1 M LiCl in DMSO	2	0.4	0.42	7	200	189
e	0.0375 M LNMO in 2-propanol	3	2	2.08	2	350	82.5
f	0.0375 M LNMO in 2-propanol	3	2	2.08	2	100	82.5
g	0.3 M LNMO in 2-propanol	3	0.5	0.74	3	200	82.5
h	0.05 M LiCl in DMSO	3	0.4	0.73	1	200	189